Particle Accelerators, 1990, Vol. 25, pp. 183–199
Reprints available directly from the publisher
Photocopying permitted by license only

Printed in the United States of America

IMPEDANCES OF A SET OF CYLINDRICAL RESONATORS WITH BEAM PIPES

H. HENKE
CERN, Geneva, Switzerland

(Received November 23, 1987)

The coupling impedances are derived for a point charge traveling parallel to the axis of an infinite pipe that is loaded with a finite number of cylindrical resonators or radial lines. The field problem is solved with a mode-matching technique, using a source field, plus a continuous spectrum of waveguide modes in the pipe region, and a discrete set of modes in the resonator regions. It is found that the longitudinal impedance in the case of a radial line shows resonant enhancement up to frequencies of a few times the pipe cut-off, then decays quickly, and seems to behave like $f^{-1/2}$ for very high frequencies f. The impedance of a resonator consists of loss-free resonances below cutoff and more and more de-Q-ed resonances above. For very small and heavily damped resonators, an additional broad-band contribution is found. Finally, we show how the impedance changes when going from a single resonator to many resonators. The resonances are shifted in frequency and become small banded—whilst the losses stay constant—until they end up in the δ-function impedance of a periodic structure.

1. INTRODUCTION

The electromagnetic beam-environment interaction limits the performance of modern accelerators or storage rings where the beam currents are high, the bunches very short, or both. Experience has shown that even very small objects such as gaps at a vacuum flange or bellows have high transverse impedances. In the case of short bunches, as proposed for the new generation of synchrotron light sources, one is afraid of having energy losses that are too high. Hence, it is considered important to arrive at a better understanding of

(1) why the longitudinal impedance decreases much faster with the size of the object than does the transverse impedance;
(2) when results obtained for infinite periodic structures[1–6] have a reasonable physical meaning;
(3) what is the impedance above cutoff; and
(4) whether numerical codes such as TBCI[7] still work reliably in the case of tiny objects.

The present paper deals analytically with the problem of a point charge traveling parallel to the axis of an infinite pipe loaded with a finite number of cylindrical resonators or radial lines (Fig. 1). Similar problems have been treated in the past in many papers. Some considered a closed pillbox[8,9] where a discrete set of known eigenmodes exists. Others estimate the radiation from the pipe into the cavity[10] or vice versa.[11,12] In the case of an infinite periodic chain of

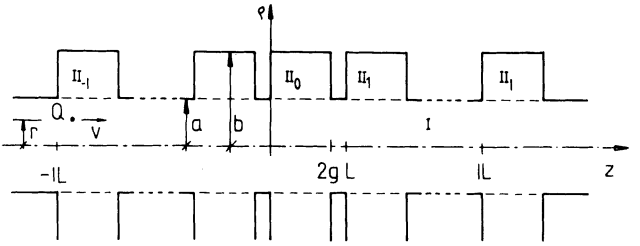

FIGURE 1 Point charge traveling parallel to the axis of an infinite pipe loaded with cylindrical resonators (upper part) or radial lines (lower part).

resonators, the fields can be decomposed into space harmonics, and a standard field-matching technique[1,2] is possible on a cylindrical surface. Instead of matching in the axial direction, a transverse plane, as proposed for a rectangular guide with a cross-section step,[13] can also be used. This procedure was later employed for a cylindrical resonator with semi-infinite beam pipes.[14–17]

The method that is applied here is also a field-matching technique with cylindrical matching interfaces, but it must use a continuous wave spectrum owing to the nonperiodicity of the problem. This approach has been used before[18,19] for a single resonator. Here it is extended to many resonators. The choice of subregions is seen to be more natural since it allows for a closed representation of the fields in the pipe region. Therefore, it yields a simple charge-field interaction integral and gives explicitly the well-known radial dependence of the interaction as well as the dependence between transverse and longitudinal impedance.

The off-axis moving charge is Fourier-decomposed into azimuthal modes, and the field problem is solved for each mode independently. For this purpose the structure is separated into subregions (Fig. 1). In the pipe (Region I) the fields consist of the source fields plus a continuous spectrum of waveguide modes. In the resonator (Regions II_i) a discrete set of radially forward and backward traveling modes is used. (In the case of radial lines, only forward traveling modes exist.) On the common interface the fields are matched, yielding an inhomogeneous set of linear equations for the expansion coefficients of the resonator region (or an integral equation for the spectrum of the pipe region). The expansion integrals that occur are solved with the residual calculus; therefore attention must be paid to the location of the poles in order to prevent waves coming in from plus or minus infinity.

2 FIELD REPRESENTATION AND MATCHING

The cylindrical coordinates ρ, φ, and z are used, and all fields are Fourier transformed; i.e., they are proportional to $\exp(j\omega t)$, which is omitted throughout the paper.

The charge Q, traveling off-axis at $\rho = r$ with constant velocity v, is Fourier-decomposed in the φ direction and Fourier-transformed in the z

direction. For the Mth component of the current density, this yields

$$\mathbf{j} = \frac{Q}{(1+\delta_M^0)\pi r} \cos M\varphi\, \delta(\rho - r) \exp(-jkz/\beta)\mathbf{e}_z, \tag{1}$$

with the wave number $k = \omega/c_0$ and $\beta = v/c_0$. Since the structure is axis symmetric, all fields will have the same azimuthal dependence as the excitation equation [Eq. (1)], and we can solve for each M independently. Therefore, all expressions given in the following belong to fields with an azimuthal mode number M.

2.1. *Source Fields in the Pipe, Region I*

Source fields are the fields in an infinitely long pipe excited by the current density [Eq. (1)]. They are well known and can be written, for $\rho > a$, as

$$\begin{aligned} H_\varphi^s &= -\frac{Qk}{(1+\delta_M^0)\pi\,|\beta|\,\gamma} \cos M\varphi\, R'(\rho) \exp(-jkz/\beta), \\ H_z^s &= 0, \\ E_\varphi^s &= \frac{QZ_0 M}{(1+\delta_M^0)\pi\beta} \sin M\varphi \frac{1}{\rho} R(\rho) \exp(-jkz/\beta), \\ E_z^s &= j\frac{QZ_0 k}{(1+\delta_M^0)\pi\beta^2\gamma^2} \cos M\varphi R(\rho) \exp(-jkz/\beta), \end{aligned} \tag{2}$$

with $\gamma = (1-\beta)^{-1/2}$, $Z_0 = (\mu_0/\varepsilon_0)^{1/2}$,

$$R(\rho) = I_M\left(\frac{kr}{|\beta|\,\gamma}\right)\left[K_M\left(\frac{k\rho}{|\beta|\,\gamma}\right) - I_M\left(\frac{k\varphi}{|\beta|\,\gamma}\right)K_M\left(\frac{ka}{|\beta|\,\gamma}\right)\Big/ I_M\left(\frac{ka}{|\beta|\,\gamma}\right)\right].$$

2.2. *Scattered Fields in the Pipe, Region I*

Because of the inhomogeneous boundary, the scattered fields must be a superposition of E- and H-waves (for $M = 0$, only E-waves are needed):

$$\begin{aligned} \mathbf{E} &= \nabla \times B\mathbf{e}_z - \frac{j}{k} Z_0 \nabla \times \nabla \times A\mathbf{e}_z, \\ \mathbf{H} &= \nabla \times A\mathbf{e}_z + \frac{j}{k} Z_0^{-1} \nabla \times \nabla \times B\mathbf{e}_z, \end{aligned} \tag{3}$$

where the vector potentials A and B are given by a continuous spectrum of waves, since there are no boundary conditions. The region is unbound in the z direction, and the fields are unknown at $\rho = a$. The only requirement is regularity at $\rho = 0$. So we have to sum over all radial (K) or longitudinal (k_z) wave

numbers. We choose k_z, yielding

$$\begin{Bmatrix} A^{\mathrm{I}} \\ B^{\mathrm{I}} \end{Bmatrix} = \int_{-\infty}^{\infty} \begin{Bmatrix} \cos M\varphi\, F(k_z) \\ Z_0 \sin M\varphi\, G(k_z) \end{Bmatrix} J_M(K\rho) \exp(-jk_z z)\, dk_z, \tag{4}$$

with $K^2 = k^2 - k_z^2$.

2.3. *Scattered Fields in the Resonator Regions II_i*

In the resonator, regions II_i, ($\rho \geq a$, $iL \leq z \leq iL + 2g$, $-I \leq i \leq I$) we use (as for the pipe region) both E- and H-waves for $M \geq 1$. But now boundary conditions exist in the z direction:

$$E_{\varphi}^{\mathrm{II}_i}(z = iL,\ iL + 2g) = 0, \tag{5}$$

and radially we find outgoing waves in the case of radial lines, and outgoing as well as incoming waves with

$$E_z^{\mathrm{II}_i}(\rho = b) = 0 \tag{6}$$

in the case of resonators. The corresponding vector potentials can then be written as

$$\begin{aligned} A^{\mathrm{II}_i} &= \cos M\varphi \sum_n A_n^i R_n(\rho) \cos k_{zn}(z - iL), \\ B^{\mathrm{II}_i} &= Z_0 \sin M\varphi \sum_n B_n^i P_n(\rho) \sin k_{zn}(z - iL), \end{aligned} \tag{7}$$

with

$$\left.\begin{aligned} R_n(\rho) &= N_M(K_n b) J_M(K_n \rho) - J_M(K_n b) N_M(K_n \rho) \\ P_n(\rho) &= N'_M(K_n b) J_M(K_n \rho) - J'_M(K_n b) N_M(K_n \rho) \end{aligned}\right\} \quad \text{for resonators,}$$

$$R_n(\rho) = P_n(\rho) = H_M^{(2)}(K_n \rho) \quad \text{for radial lines,}$$

with $K_n^2 = k^2 - k_{zn}^2$, and $k_{zn} = n\pi/2g$.

2.4. *Matching of the Electric field*

In Region I, the complete solution is given by the source fields [Eq. (2)], plus the scattered fields [Eqs. (3) and (4)], whereas in Region II_i only scattered fields [Eqs. (3) and (7)] are present. Then, at the interface $\rho = a$, the continuity condition can be written as

$$E_p^s + E_p^{\mathrm{I}} = \begin{cases} E_p^{\mathrm{II}_i} & \text{for } iL \leq z \leq iL + 2g, \\ 0 & \text{elsewhere,} \end{cases} \tag{8}$$

where the subscript p stands for z or φ.

Multiplying Eq. (8) with $\exp(jk'_z z)$ and integrating over z, we find

$$\int_{-\infty}^{\infty} (E_p^s + E_p^{\mathrm{I}}) \exp(jk'_z z)\, dz = \sum_i \int_{iL}^{iL+2g} E_p^{\mathrm{II}_i} \exp(jk'_z z)\, dz. \tag{9}$$

The integrals on the right-hand side can easily be performed. For the left-hand side we use the identity

$$\int_{-\infty}^{\infty} \exp[j(k'_z - k_z)z]\, dz = 2\pi\delta(k'_z - k_z). \tag{10}$$

Consequently, we find the spectral functions F and G expressed in sums over A_n^i and B_n^i:

$$\begin{aligned} 2\pi F(k_z)K^2 J_M(Ka) &= \sum_n K_n^2 R_n(a) \sum_i A_n^i C_n^i(k_z) \\ 2\pi\left[\frac{M}{ka} F(k_z)k_z J_M(Ka) - G(k_z)K J'_M(Ka)\right] & \\ = -j\frac{M}{ka} \sum_n k_{zn} R_n(a) \sum_i A_n^i S_n^i(k_z) - \sum_n P'_n(a) \sum_i B_n^i S_n^i(k_z). & \end{aligned} \tag{11}$$

The expressions C and S are integrals over z and are given in Appendix A.

2.5. Matching of the Magnetic Field

After having derived the magnetic fields from the vector potentials [Eq. (4)], we introduce the spectral functions F and G, Eq. (11), and obtain the field of region I expressed by the coefficients A_n^i and B_n^i of Region II_i. The integrals that occur are solved by means of the residual calculus (see appendix B); thereby attention must be paid to the location of the poles. They must be placed so that for a lossy structure the waves excited at the input and output ports, $z = -IL$ and $z = IL + 2g$, respectively, are damped and travel away from the structure.

In contrast to the electric fields, the tangential magnetic fields are unknown on the pipe walls. On the interfaces, $\rho = a$, $iL \le z \le iL + 2g$, they must be continuous:

$$H_p^s + H_p^{\mathrm{I}} = H_p^{\mathrm{II}_i}, \qquad p = z, \varphi. \tag{12}$$

In this case we expand the fields of the Regions II_i in terms of the functions of Region I; i.e.,

$$\int_{iL}^{iL+2g} H_z^{\mathrm{I}} \sin k_{zm}(z - iL)\, dz = \int_{iL}^{iL+2g} H_z^{\mathrm{II}_i} \sin k_{zm}(z - iL)\, dz,$$

$$\int_{iL}^{iL+2g} (H_\varphi^s + H_\varphi^{\mathrm{I}}) \cos k_{zm}(z - iL)\, dz = \int_{iL}^{iL+2g} H_\varphi^{\mathrm{II}_i} \cos k_{zm}(z - iL)\, dz,$$

yielding

$$2\pi(1-\delta_M^0)gK_M^2P_m(a)B_m^i = jM\frac{k}{a}\sum_n\sum_i K_n^{-2}I_{nm}^{(1)}A_n^i - \sum_n\sum_i k_{zn}P_n(a)I_{nm}^{(2)}B_n,$$

$$\begin{aligned}2\pi(1+\delta_M^0)g\left[\frac{jM}{ka}k_{zm}P_m(a)B_m^i - R_m'(a)A_m^i\right] &= \frac{-QkR'(a)}{(1+\delta_M^0)\pi\,|\beta|\,\gamma}C_m^i(-k/\beta) - j\sum_n\sum_i\left[I_{nm}^{(3)} - \frac{M^2}{K_n^2a^2}I_{nm}^{(4)}\right]A_n^i \\ &\quad - \frac{M}{ka}\sum_n\sum_i k_{zn}P_n(a)I_{nm}^{(5)}B_n^i.\end{aligned} \tag{13}$$

Equations (13) are a system of linear equations for the expansion coefficients A_n^i and B_n^i. They can be solved after truncation. The constants $I_{nm}^{(i)}$, $i = 1, \ldots, 5$, are expansion integrals and are derived in Appendix B.

Alternatively, we could use the condition of Eq. (12) directly, before substituting F and G from Eq. (11) into Eq. (4). This means that we express A_n^i and B_n^i in terms of F and G and substitute them into Eq. (11). Then we obtain two coupled integral equations that may be more suitable for deriving approximations or asymptotic behaviour.

3. DERIVATION OF THE COUPLING IMPEDANCES

The longitudinal and transverse coupling impedances are defined as

$$\begin{aligned}Z_L(\omega) &= -\frac{1}{Qr^Mr_1^M\cos M\varphi_1}\int_{-\infty}^{\infty}E_z^{\mathrm{I}}\exp(jkz/\beta)\,dz, \\ Z_T(\omega) &= -\frac{j}{Qr^Mr_1^{M-1}\cos M\varphi_1}\int_{-\infty}^{\infty}(E_\rho^{\mathrm{I}} - \mu_0 v H_\varphi^{\mathrm{I}})\exp(jkz/\beta)\,dz,\end{aligned} \tag{14}$$

where the integration is performed along a path ($\rho = r_1$, $\varphi = \varphi_1$). They are normalized so that for relativistic particles they are independent of the position ($\rho = r$, $\varphi = 0$) of the exciting charge and the position ($\rho = r_1$, $\varphi = \varphi_1$) of the probing charge.

Substituting the fields from Eqs. (3) and (4), and using Eqs. (10) and (11), one obtains for the impedances [Eq. (14)],

$$\begin{aligned}Z_L(\omega) &= j\frac{Z_0}{Qr^Mr_1^M}\frac{1}{k}\lim_{k_z\to k/\beta}2\pi F(k_z)K^2J_M(Kr_1) \\ &= j\frac{Z_0}{Qr^Mr_1^M}\frac{1}{k}\frac{I_M(\sqrt{\beta^{-2}-1}\,kr_1)}{I_M(\sqrt{\beta^{-2}-1}\,ka)}\sum_n K_n^2R_n(a)\sum_i C_n^i(k/\beta)A_n^i, \\ Z_T(\omega) &= r_1\beta\sqrt{\beta^{-2}-1}\,\frac{I_M'(\sqrt{\beta^{-2}-1}\,kr_1)}{I_M(\sqrt{\beta^{-2}-1}\,kr_1)}Z_L(\omega),\end{aligned} \tag{15}$$

which in the case of relativistic motion becomes

$$Z_L(\omega) = \frac{jZ_0}{Qkr^M a^M} \sum_n K_n^2 R_n(a) \sum_i C_n^i(k) A_n^i,$$
$$Z_T(\omega) = \frac{M}{k} Z_L(\omega). \tag{16}$$

Equations (16) show the well-known relation between the longitudinal and the transverse impedance of the same azimuthal mode M.

4. NUMERICAL RESULTS

Apart from some special cases such as short gap length or low frequency, where approximate formulae can be derived, the system of linear equations [Eqs. (13)] must be solved. For this purpose a computer code ICYRP (Impedances of Cylindrical Resonators with Pipes) has been written. It truncates the system to an order $n + n_1$, where n corresponds to $k_{zn} \approx k$, and n_1 is typically between 1 and 10.

As a first example let us consider the longitudinal impedance of a radial line (Fig. 2). Here the impedance is dominated by the radiation into the radial line and does not show resonant behaviour as for a cavity. The real part of the impedance increases rapidly from zero frequency onward (there is no cutoff in the radial line), reaches a maximum around $2g \approx \lambda/2$, and decays. At each cutoff frequency $k_c = k_{zn}$ of the radial line, a new mode starts propagating, and the

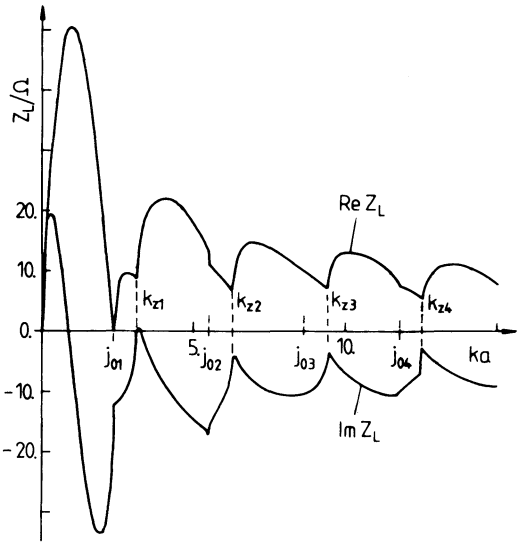

FIGURE 2 Longitudinal impedance of a radial line (geometry of Fig. 1 with $I = 0$, $a = 2g = 15$ mm, $\gamma = 10^6$).

impedance increases correspondingly. This example is also better suited to the study of the high-frequency behaviour than is a resonator. At first, we can excite only even or odd modes when selecting the cutoff values $k = k_{zn}$. This means that the system [Eq. (13)] reduces to half the order, and we can go up to twice the frequency. Secondly, the behaviour is smoother than for a resonator and allows a direct visualization of the decay with frequency. Figure 3 shows the real part of the longitudinal impedances at selected high-frequency points equal to $k = k_{zn}$ for various gap widths. For 15-, 30-, and 60-mm gaps, the impedance clearly seems to decay with $\omega^{-1/2}$. For the 120-mm gap, we could not yet reach the high-ω region, although $ka = 40$ means that there are about 100 modes taken into account in Region II. The impedance is still in a range were interference plays a role.

In a resonator (Fig. 4) the situation is quite different. Radiation can occur only into the pipes with a cutoff frequency of $ka = j_{01} = 2.405$. Below the cutoff the impedance shows loss-free resonances. The real part is zero, apart from resonances, where it consists of δ-functions. The imaginary part behaves like a reactance. Above cutoff, the resonances are no longer loss free owing to the radiation into the pipe. Some modes are still well trapped; others are heavily degraded. In Table I we make a comparison between modes of a closed pillbox and the resonator with pipes (Fig. 4). The modes (0, 0, 1), (0, 0, 2), and (0, 1, 1) are well conserved and shifted only slightly up in frequency. The higher modes (0, 1, 2) and (0, 1, 3) are shifted quite a lot owing to the beam ports; this corresponds to a reduction of the capacitance. Other modes are so strongly Q-degraded that they are either barely seen or are not seen at all, as for modes (0, 0, 3) and (0, 0, 4), respectively. Finally, it should be mentioned that even for very high frequencies the impedance behaves quite irregularly, as indicated in Fig. 4. A study of the ω dependence would therefore require integration over bins—a

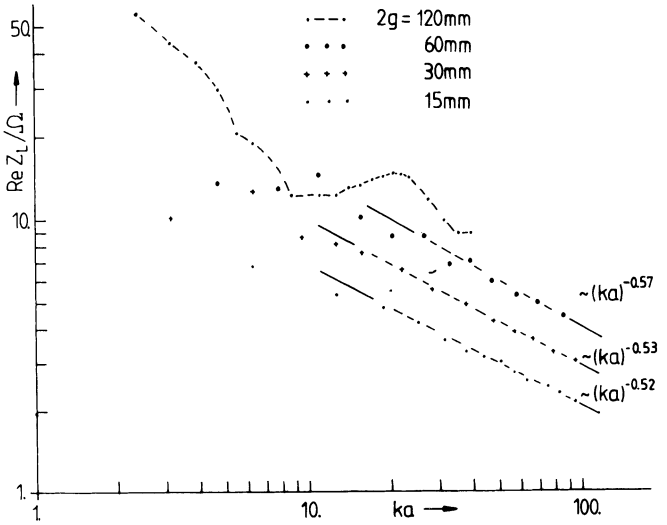

FIGURE 3 High-frequency dependence of the longitudinal impedance of radial lines (geometry of Fig. 1 with $I = 0$, $a = 15$ mm, $\gamma = 10^6$).

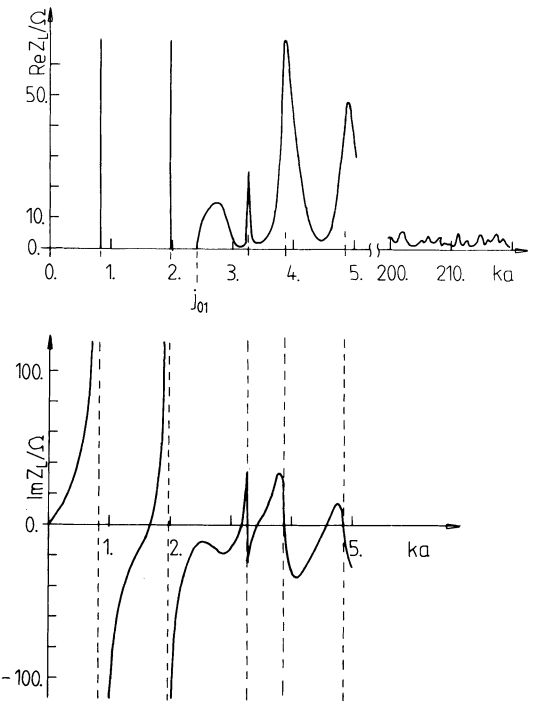

FIGURE 4 Longitudinal impedance ($M = 0$) of a cylindrical resonator (geometry of Fig. 1 with $I = 0$, $a = 2g = 15$ mm, $d = 30$ mm, $\gamma = 10^6$).

TABLE I

Resonant modes of closed and open resonators:

$a = 2g = 15$ mm, $b = 45$ mm.

Closed resonator; $(ka)_{mnp} = [(n\pi a/2g)^2 + (j_{mp}a/b)^2]^{1/2}$

m	n	p	$(ka)_{mnp}$	ka open resonator (Figs. 4 and 5)
0	0	1	0.802	0.82
0	0	2	1.840	1.97
0	0	3	2.885	Hidden
0	1	1	3.242	3.27
0	1	2	3.641	3.86
0	0	4	3.930	Hidden
0	1	3	4.265	4.85
1	0	1	1.277	1.22
1	1	1	3.391	1.78
1	0	2	2.339	2.31
1	1	2	3.916	3.28
1	0	3	3.391	3.48
1	1	3	4.623	3.85

possible way, but it consumes more computer time than the procedure chosen above for the radial line.

In Fig. 5 the transverse impedance $M = 1$ is given for the same cavity (Fig. 4). As in the longitudinal case, the impedance is imaginary below cutoff of the lowest TE mode, $ka = j'_{11} = 1.841$. The real part consists of δ-functions. Above cutoff the resonances are Q-degraded. Since for transverse modes the fields are essentially magnetic in the pipe region, the aperture corresponds to an increase of the inductance and, therefore, a decrease of resonant frequencies, as can be seen from Table I. We also see that the frequency shift is much more pronounced than for the longitudinal resonances.

The next example is a very small resonator corresponding, for instance, to one undulation of a bellows used as the compensation element in the vacuum pipe (Fig. 6). Apparently, the impedance consists of three parts. A broad-band resonance at $ka = 12.8$ with a Q of 5. This corresponds to a resonance on a radial line of length $d \approx \lambda/4$, which is heavily damped by radiation into the pipe. In series with the broad-band impedance, we find several high-Q resonances (in this case, four) belonging to well-trapped modes. Finally, there are notches located at $ka = j_{0s}$, the cutoff frequencies of the pipe. They result because, for $\lambda \ll 2g$, only

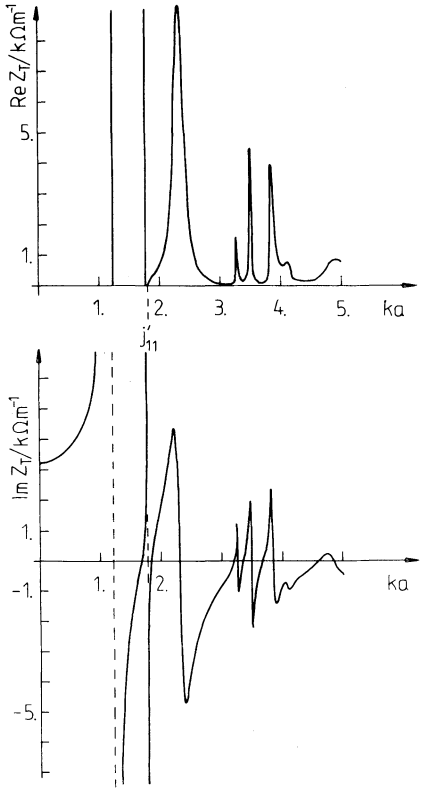

FIGURE 5 Transverse impedance ($M = 1$) of the resonator in Fig. 4.

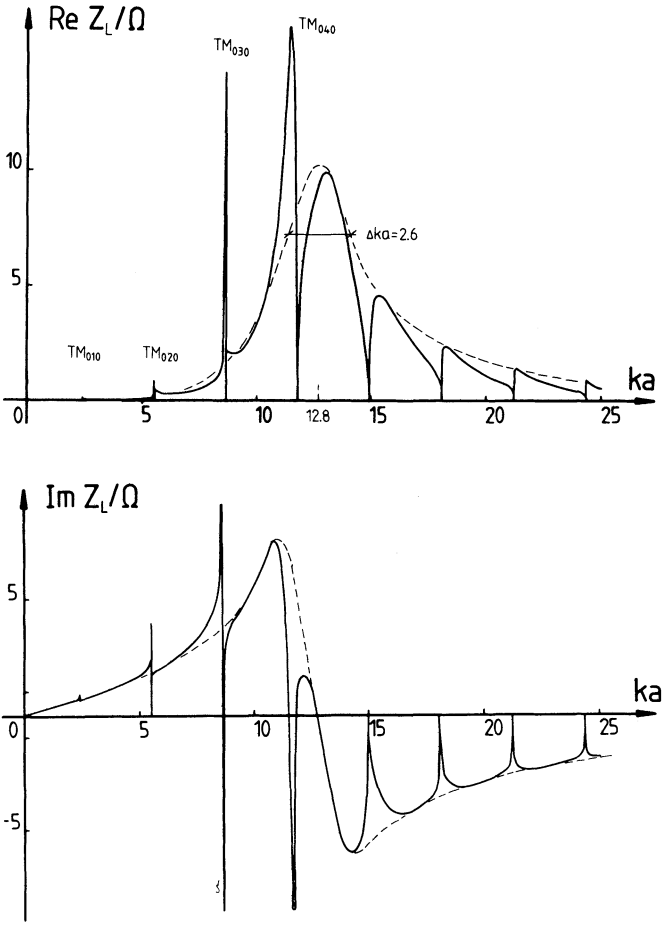

FIGURE 6 Longitudinal impedance ($M = 0$) of a small cylindrical resonator (geometry of Fig. 1 with $I = 0$, $a = 40$ mm, $2g = 2$ mm, $d = 4$ mm, $\gamma = 10^6$).

the z-independent mode exists in the resonator region, but it is not excited since $E_z^I(\rho = a) = 0$. There are no secondary fields at cutoff.

The transverse impedance ($M = 1$) for the resonator in Fig. 6 is given in Fig. 7. It looks very similar to the longitudinal impedance; the main difference is the nonzero imaginary part for low frequencies. Note that the transverse impedance in Fig. 3 of Ref. 18 is wrong, apart from the different definition with a negative sign as used here [Eq. (14)].

As a last example, we will treat the transition from a single undulation of a bellows to an infinite periodic structure. Figure 8 shows the real part of the longitudinal impedance for an increasing number of undulations. As in the foregoing example, the single undulation has a broad-band resonance that is located at $ka = 4.7$ in this case. This corresponds to a $\lambda/4$ resonance of the radial

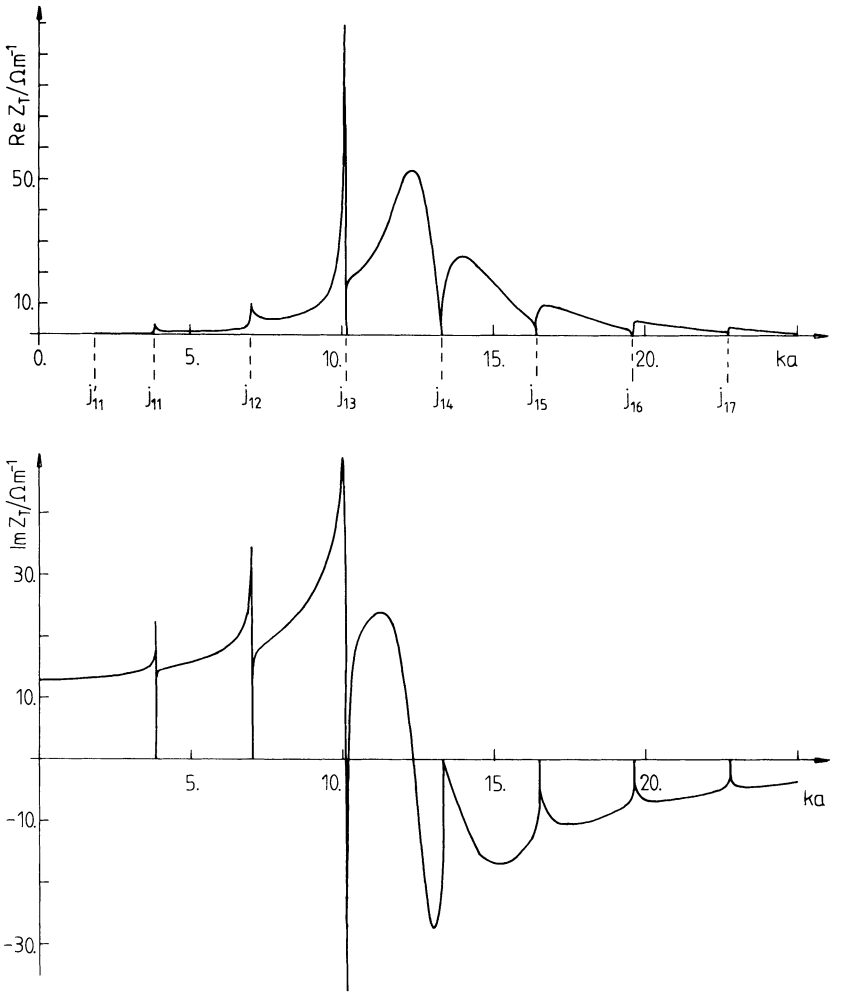

FIGURE 7 Transverse impedance ($M = 1$) of the resonator in Fig. 6.

line. With increasing number of undulations the resonance at first becomes broader, owing to coupling between undulations, and is shifted in frequency. For more than 20 undulations, a real isolated resonance is formed at $ka = 3.45$. This resonance becomes smaller and smaller in bandwidth, although the losses per undulation stay constant. In Fig. 9 it is depicted for 41 undulations, for instance. Note the highly suppressed losses outside the transmission band $ka = 3.2$ through $ka = 3.8$. Finally, the resonance becomes δ-function-like for the case of an infinite periodic structure. The resonance frequency $ka = 3.45$ is that of the space harmonic, which has a phase velocity equal to the velocity of light in the first passband (Fig. 10).

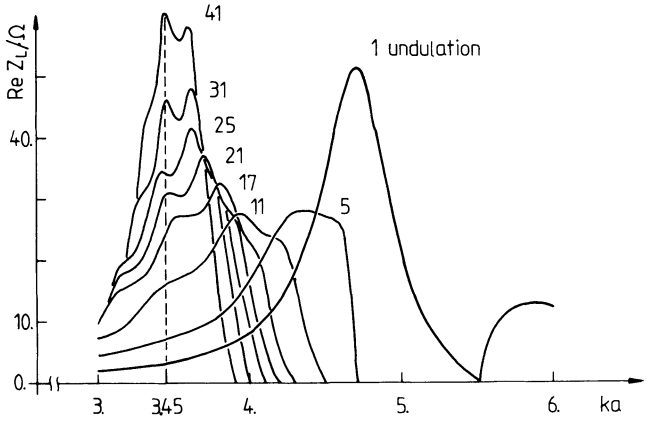

FIGURE 8 Real part of the longitudinal impedance of a set of cylindrical resonators (geometry of Fig. 1 with $a = 15$ mm, $2g = 2$ mm, $d = L = 4$ mm, $\gamma = 10^6$).

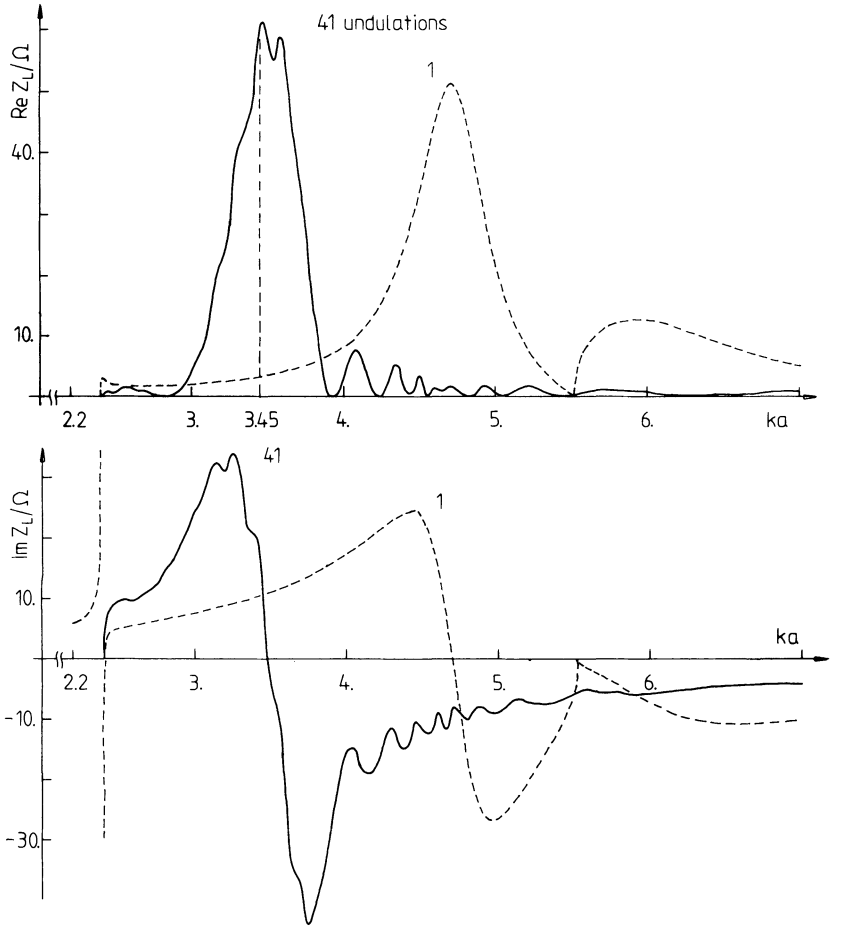

FIGURE 9 Longitudinal impedance of a set of 41 cylindrical resonators as shown in Fig. 8.

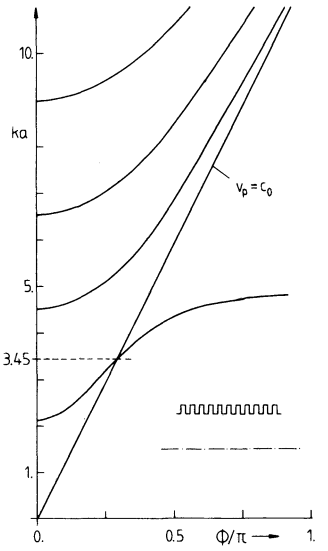

FIGURE 10 Brillouin diagram of the first passbands in an infinite periodic structure of cylindrical resonators. Dimensions as in Fig. 8.

REFERENCES

1. E. Keil, *Proc. 7th Int. Conf. on High-Energy Accelerators,* Yerevan, 1969, vol. II, pp. 551–560.
2. E. Keil and B. Zotter, *Part. Acc.* **3,** 11 (1972).
3. M. Chatard-Moulin and A. Papiernik, *IEEE Trans. Nucl. Sci.* **NS-26,** 3523 (1979).
4. S. Krinsky, *Proc. 11th Int. Conf. on High-Energy Accelerators,* Geneva, 1980 (Birkhäuser Verlag, Basle, 1980), pp. 576–580.
5. R. K. Cooper, S. Krinsky, and P. L. Morton, *Part. Acc.* **12,** 1 (1982).
6. S. Kheifets and B. Zotter, CERN, internal report CERN/LEP-TH/85-27 (1985).
7. T. Weiland, *Nucl. Instrum. Methods* **212,** 13 (1983).
8. P. L. Morton and V. K. Neil, *Proc. Symp. on Electron Ring Accelerators,* Berkeley, 1968, Lawrence Berkeley Laboratory report UCRL-18103, pp. 365–375, (1968).
9. E. Keil, C. Pellegrini, and A. M. Sessler, *Nucl. Instrum. Methods* **127,** 475 (1975).
10. J. D. Lawson, Rutherford Lab. internal report RHEL/M 144 (1968).
11. O. A. Kolpakov and V. I. Kotov, *Sov. Phys.-Tech. Phys.* **9,** 1072 (1965).
12. G. Dôme, *IEEE Trans. Nucl. Sci.* **NS-32,** 2531 (1985).
13. H. G. Hereward, CERN internal report CERN/ISR-DI/75-47 (1975).
14. H. Hahn and S. Zatz, *IEEE Trans. Nucl. Sci.* **NS-26,** 3626 (1975).
15. L. Vos, CERN internal report CERN-SPS/86-21 (MS) (1986).
16. S. Kheifets, Stanford Linear Accelerator Center internal report SLAC-PUB-4133 (1986).
17. S. A. Kheifets, K. L. F. Bane, and H. Bizek, Stanford Linear Accelerator Center internal report SLAC-PUB-4097 (1987).
18. H. Henke, *IEEE Trans. Nucl. Sci.* **NS-32,** 2335 (1985).
19. H. Henke, CERN internal report CERN/LEP-RF/85-41 (1985).
20. H. Buchholz, Z. Angew. *Math. & Mech.* **25/27** Nr. 8/9, 245 (1947).

APPENDIX A

The integrals in Eq. (11) are

$$\begin{Bmatrix} C_n^i(k_z) \\ S_n^i(k_z) \end{Bmatrix} = \int_{iL}^{iL+2g} \begin{Bmatrix} \cos \\ \sin \end{Bmatrix} [k_{zn}(z - iL)] e^{jk_z z}\, dz$$

$$= \begin{Bmatrix} jk_z \\ -k_{zn} \end{Bmatrix} \frac{1}{k_z^2 - k_{zn}^2} [1 - e^{jn\pi} e^{j2k_z g}] e^{jik_z L}. \tag{A-1}$$

APPENDIX B

The expansion integrals $I_{nm}^{(i)}$, $i = 1, \ldots, 5$, in Eq. (13) are given by

$$I_{nm}^{(i)} = \int_{iL}^{iL+2g} i_n^{(i)} \sin k_{zm}(z - iL)\, dz \qquad \text{for } i = 1, 2,$$

$$I_{nm}^{(i)} = \int_{iL}^{iL+2g} i_n^{(i)} \cos k_{zm}(z - iL)\, dz \qquad \text{for } i = 3, 4, 5, \tag{B-1}$$

where the integrands $i_n^{(i)}$ follow from introducing F and G [Eq. (11)] into the expression for the magnetic fields in region I. These integrands can be written as (all length quantities normalized with respect to a)

$$i_n^{(1)}(z) = \int_{-\infty}^{\infty} \varphi(k_z, z) \frac{J_M(K)}{KJ'_M(K)}\, dk_z,$$

$$i_n^{(2)}(z) = \int_{-\infty}^{\infty} \varphi(k_z, z) \frac{K^2}{k_z^2 - k_{zn}^2} \frac{J_M(K)}{KJ'_M(K)}\, dk_z,$$

$$i_n^{(3)}(z) = \int_{-\infty}^{\infty} \varphi(k_z, z) \frac{k_z}{k_z^2 - k_{zn}^2} \frac{J'_M(K)}{KJ_M(K)}\, dk_z, \tag{B-2}$$

$$i_n^{(4)}(z) = \int_{-\infty}^{\infty} \varphi(k_z, z) \frac{k_z}{K^2} \frac{J_M(K)}{KJ'_M(K)}\, dk_z,$$

$$i_n^{(5)}(z) = \int_{-\infty}^{\infty} \varphi(k_z, z) \frac{k_z}{k_z^2 - k_{zn}^2} \frac{J_M(K)}{KJ'_M(K)}\, dk_z,$$

with

$$K^2 = k^2 - k_z^2$$

and

$$\varphi(k_z, z) = e^{jk_z(iL - z)} - e^{jn\pi} e^{jk_z(iL + 2g - z)}.$$

The ratios of Bessel functions can be expanded in series:[20]

$$\frac{J_M(K)}{KJ'_M(K)} = -\frac{2}{K^2}\delta_M^0 + 2\sum_s \frac{j'^2_{Ms}}{j'^2_{Ms}-M^2}\frac{1}{k_z^2-b_s'^2}$$
$$\frac{J'_M(K)}{KJ_M(K)} = \frac{M^2}{K^2} - 2\sum_s \frac{1}{k_z^2-b_s^2} \qquad \text{(B-3)}$$

with

$$b_s = \begin{cases} \beta_s = \sqrt{k^2 - j_{Ms}^2} \\ -j\alpha_s = -j\sqrt{j_{Ms}^2 - k^2} \end{cases} \qquad b'_s = \begin{cases} \beta'_s = \sqrt{k^2 - j'^2_{Ms}} \\ -j\alpha'_s = -j\sqrt{j'^2_{Ms} - k^2} \end{cases} \qquad \text{for} \begin{cases} k \geq j_{Ms}, j'_{Ms} \\ k < j_{Ms}, j'_{Ms} \end{cases}.$$

After introducing Eq. (B-3) into Eq. (B-2), the integrands $i_n^{(n)}(z)$ can all be expressed in terms of the following integral:

$$I(\alpha, \beta, z) = \int_{-\infty}^{\infty} \frac{\exp[jk_z(iL - z)]}{(k_z^2-\alpha^2)(k_z^2-\beta^2)}\,dk_z - e^{jn\pi}\int_{-\infty}^{\infty} \frac{\exp[jk_z(iL + 2g - z)]}{(k_z^2-\alpha^2)(k_z^2-\beta^2)}\,dk_z, \qquad \text{(B-4)}$$

which is solved by means of the residual calculus. The integration paths and the poles, shown in Fig. 11, are thereby chosen so that the modes excited at the input and output ports, $z = -IL$ and $z = IL + 2g$, respectively, are damped and travel away from the structure. This results in

$$I(\alpha, \beta, z) = \frac{j\pi}{\alpha^2-\beta^2}\left\{\frac{1}{\beta}[\psi_1(\beta, z) - \psi_2(\beta, z)] - \frac{1}{\alpha}[\psi_1(\alpha, z) - \psi_2(\alpha, z)]\right\},$$
$$I'(\alpha, \beta, z) = \frac{\pi}{\alpha^2-\beta^2}[\psi_1(\beta, z) + \psi_2(\beta, z) - \psi_1(\alpha, z) - \psi_2(\alpha, z)], \qquad \text{(B-5)}$$
$$I''(\alpha, \beta, z) = \frac{j\pi}{\alpha^2-\beta^2}\{\alpha[\psi_1(\alpha, z) - \psi_2(\alpha, z)] - \beta[\psi_1(\beta, z) - \psi_2(\beta, z)]\},$$

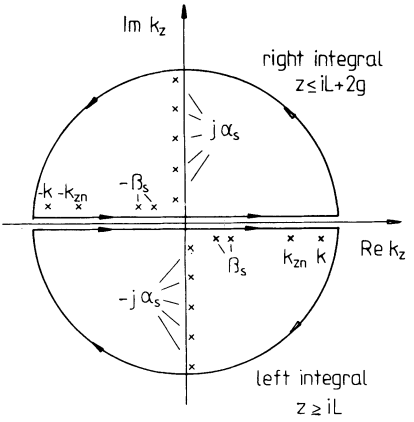

FIGURE 11 Integration path and location of poles in the k_z plane.

with

$$\psi_1(\alpha, z) = \exp[j\alpha(iL - z)],$$

$$\psi_2(\alpha, z) = \exp(jn\pi)\exp[-j\alpha(iL + 2g - z)].$$

Using Eq. (B-5) in Eq. (B-2) we can write

$$i_n^{(1)}(z) = -2\delta_M^0 I''(k, 0, z) - 2\sum_s \frac{j_{Ms}'^2}{j_{Ms}'^2 - M^2} I''(b_s', 0, z),$$

$$i_n^{(2)}(z) = 2\delta_M^0 I''(k_{zn}, 0, z) + 2\sum_s \frac{j_{Ms}'^2}{j_{Ms}'^2 - M^2}[k^2 I(k_{zn}, b_s', z) + I''(k_{zn}, b_s', z)]$$

$$i_n^{(3)}(z) = -jM^2 I'(k_{zn}, k, z) - j2\sum_s I'(k_{zn}, b_s, z), \tag{B-6}$$

$$i_n^{(4)}(z) = -j2\delta_M^0 I'(k, k, z) - j2\sum_s \frac{j_{Ms}'^2}{j_{Ms}'^2 - M^2} I'(k, b_s', z),$$

$$i_n^{(5)}(z) = j2\delta_M^0 I'(k_{zn}, k, z) + j2\sum_s \frac{j_{Ms}'^2}{j_{Ms}'^2 - M^2} I'(k_{zn}, b_s', z).$$

The remaining integration over z [Eq. (B-1)] is straightforward and gives the expressions of Eq. (A1).